IEEE Access
Multidisciplinary ⋮ Rapid Review ⋮ Open Access Journal

Received November 24, 2021, accepted January 27, 2022, date of publication February 18, 2022, date of current version February 28, 2022.

Digital Object Identifier 10.1109/ACCESS.2022.3151722

A 1.55 μm Wideband 1 × 2 Photonic Power Splitter With Arbitrary Ratio: Characterization and Forward Modeling

LUBABA TAZRIAN RAHMAN[1], MAHMUD ELAHI AKHTER[2], FAIZUL RAKIB SAYEM[1], MAINUL HOSSAIN[1], (Member, IEEE), RAJIB AHMED[3], M. M. LUTFE ELAHI[2], KHALEDA ALI[1], AND SHARNALI ISLAM[1]

[1]Department of Electrical and Electronic Engineering, University of Dhaka, Dhaka 1000, Bangladesh
[2]Department of Electrical and Computer Engineering, North South University, Dhaka 1229, Bangladesh
[3]School of Medicine, Stanford University, Palo Alto, CA 94304, USA

Corresponding author: Sharnali Islam (sharnali.eee@du.ac.bd)

This work was supported by the Centennial Research Grant, University of Dhaka.

ABSTRACT Chip-based photonic systems have undergone substantial progress over the last decade. However, the realization of photonic devices still depends largely on intuition-based trial-and-error methods, with a limited focus on characteristic analysis. In this work, we demonstrate an in-depth investigation of photonic power splitters by considering the transmission properties of 16,000 unique ultra-compact silicon-based structures engraved with SiO_2, Al_2O_3, and Si_3N_4 nanoholes. The characterization has been performed using finite-difference time-domain (FDTD) simulations for each dielectric material and both TE and TM polarizations at the fundamental modes in a wideband optical communication spectrum ranging from 1.45 to 1.65 μm. The corresponding transmissions, splitting ratio, and reflection loss were calculated, generating a dataset that can be used for both forward and inverse modeling purposes, using Machine Learning (ML) and Deep Learning (DL) algorithms. With an optimized hole radius of 35 nm, the proposed device area footprint of 2 μm × 2 μm is among the smallest with the best transmission reported to date. Si_3N_4 holes show excellent transmission because they offer 90% transmittance in 96% of the data while exhibiting maximum fabrication tolerance. Forward modeling analysis, predicting the transmission properties, was performed using both Linear Model (LM) and Artificial Neural Network (ANN), where LM showed marginally better accuracy than ANN in foreseeing the transmittance. The proposed observation will aid in achieving robust, optimized optical power splitters with a wide range of splitting ratios in lesser time.

INDEX TERMS Forward modeling, machine learning, optical power splitter, artificial neural network.

I. INTRODUCTION

Recent advances in fabrication techniques have enabled ultra-scaling of both optical and electronic devices [1]. Especially, the last decade has seen a significant push towards integrated optical circuits and devices [2]. A plethora of probable application areas [3]–[7] has been demonstrated leveraging the benefits of nanoscale photonic devices. The primary motivation is that the same amount of data can be handled using much less amount of power with optical signals compared to electronic ones.

One of the primitive components for integrated optics involves optical interconnects [8] and photonic power splitters are a significant member of the interconnect family [9]. A good photonic splitter can direct the light input of a certain wavelength to multiple ports at varying intensities with minimum losses. These passive devices may lend themselves to applications ranging from signal distribution [10], [11], feedback circuits [12], to power equalization [13], or even in-mode multiplexers [14]. Popular designs of photonic power splitters [15]–[18] include a symmetrical pattern of silica or uniform distribution of pores etched onto the silicon substrate for guiding the electromagnetic wave [14], [19]. Unfortunately, these simple, yet easily conceivable structures are bound to explore only a limited number of architectures.

The associate editor coordinating the review of this manuscript and approving it for publication was Yang Yue.

This work is licensed under a Creative Commons Attribution 4.0 License. For more information, see https://creativecommons.org/licenses/by/4.0/

Hence, a broad range of transmittance ratios at the output ports remains unexplored. Having no empirical formula relating geometry, and transmission for power splitter, the analysis triggers a complex scenario. As a result, little has been known regarding the influence of materials and modes on split waves or the etched dielectric hole density and dimension optimization.

This study presents a comprehensive analysis of the characteristics of silicon-based photonic power splitters, having holes with three different dielectric materials (SiO_2, Al_2O_3 and Si_3N_4) for a 200 nm operating window keeping 1.55 μm as central wavelength. First, 16 thousand random blueprints of power splitters are generated, then their performances are simulated and finally, the results are statistically analyzed. Traditionally, securing the desired transmission requires a long iterative process, where we guess the device geometry, solve Maxwell's equations and finally achieve a design with reasonable performance. To circumvent the intuitive approach, we took the advantage of our 16 thousand training instances and applied the concept of ANN. Being universal function approximators [20], deep learners like ANNs can accurately predict the properties of the splitters [21] in any forward modeling problem. In general, these algorithms offer productive solutions as once trained, they can estimate the response accurately of any random system [22]–[24]. Other numerical and topological optimization techniques [25] or genetic algorithm [26] based methods can be employed for similar purposes. These methods, however, are expensive in terms of time and computational resources compared to Artificial Intelligence (AI)-based techniques like ML and DL. Hence, by implementing ANN in this work, we bridge the gap between characterization and performance evaluation of photonic power splitters, avoiding time-intensive and computationally exhaustive steps. This also enables us to achieve higher performance at smaller footprints with arbitrary structure, which opens up possibilities to achieve a broad range of desired responses.

To the best of our knowledge, this work is the first one to make the data pool of photonic power splitter open-sourced [27]. As AI-based solutions are currently going through a generalization crisis [28], open-source solutions and datasets are crucial to achieving more viable, robust and practical solutions.

The organization of the paper is as follows: Section II discusses the design and characterization of the photonic power splitters with respect to mode, material and hole dimensions. Section III depicts the inclusion of DNN in our current study to accurately monitor transmittance and reflection losses. Finally, Section IV concludes.

II. DESIGN METHOD AND CHARACTERIZATION

A robust photonic power splitter is mainly composed of optical branching waveguides [29], which direct the optical signals of intended power density, through the device and to the designated ports. In this work, a silicon substrate of dimension 2 μm × 2 μm area and 0.01 μm thickness has been adopted to design an optical power splitter working in the range of 1.45 to 1.65 μm. Here, T_1 and T_2 are the outputs of ports 1 and 2, respectively. Here, the transmitted outputs are estimated by keeping the power monitors at the edge of the structure. The lengths of the monitors are half of the length of the substrate. Since the monitors cover the whole length of the structure, no edge loss was required to be calculated. The total surface area is considered to be composed of 20 × 20 pixels, where each pixel corresponds to either a dielectric hole with optimized dimension or a solid. The holes are etched at different matrix positions to enable the optical wave interaction with the structure to guide the EM wave in the desired path and different combination of holes and substrate have been explored. Si as substrate material exhibits low loss at the concerned wavelength [30] and as for holes, three distinct dielectric materials are adopted: silicon dioxide (SiO_2), aluminum oxide (Al_2O_3) and silicon nitride (Si_3N_4). Relative variations of refractive indices ($\Delta\eta = \eta_{\text{substrate}} - \eta_{\text{holes}}$) between substrate and hole materials affect effective dielectric properties of the media and hence the propagation phenomena. The schematic of the structure and the dielectric properties of the constituent materials are given in Fig.1 and Table 1 respectively. In Fig. 1, the black surface represents the substrate; blue circles indicate the dielectric holes.

In this work, we have done the characterization analysis at the concerned spectrum for both fundamental transverse electric (TE) and transverse magnetic (TM) modes. Commercial FDTD based software, Lumerical has been used to perform the numerical study. Performance optimization has been done

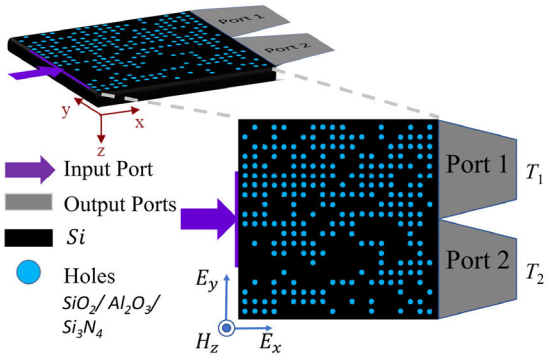

FIGURE 1. 2D and 3D schematic of a 1 × 2 nanostructured photonic power splitter with a footprint of 2 μm × 2 μm on a Silicon substrate. Circles are indicating the locations of each hole, with an optimized radius of 35 nm. A broadband light is illuminated at the input port; transmitted through the device and an output signal is collected at output ports of port 1 (T_1) and port 2 (T_2).

TABLE 1. Dielectric properties of materials at 1.5 μm wavelength.

Material	Permittivity(ε)	Refractive Index(η)
Silicon (SI)	12.1	3.48
Silicon Dioxide (SiO_2)	2.08	1.44
Aluminum Oxide (Al_2O_3)	3.05	1.75
Silicon Nitride (Si_3N_4)	6.07	2.46

in terms of hole dimension, material selection, effects of TE and TM modes on transmittance and splitting ratios and the influences of hole positions on the transmission direction by using 16 thousand unique photonic power splitters.

A. UNIQUE PATTERN GENERATION

The geometry of the hole pattern significantly *alters* the performance of the splitter. Therefore, a set of 16 thousand random patterns of holes are generated to characterize different aspects of the splitter. The whole substrate was considered to be composed of 20 × 20 array positions. A random number generating algorithm was implemented to define the values of each position as 1 or 0 arbitrarily with a 40%-60% hole occupancy in the structure. This constraint has been set to ensure a realistic power transmission scenario. The design sets are unique with random irregularities and the transmission through either port follows a normal distribution (Discussed further in section C).

B. HOLE RADIUS OPTIMIZATION

The existing literature on power splitters lacks clarity regarding the determination and optimization of the radius of the dielectric holes [31], [32]. To achieve the best performance of the power splitter, hole radii are optimized in terms of transmittance and reflectance.

First, a random distribution of holes that has a 1:1 power splitting ratio in TE mode has been chosen to be engraved onto the silicon substrate (Fig. 2(a)). The hole radii are varied from 15 nm to 90 nm at 5 nm intervals for a Gaussian source of wavelength (λ) of 1.55 μm. With the advancement of various promising nanolithography process providing high resolution, precision and low line edge error for fabrication of nanostructures, such small feature size is now made possible to fabricate with negligible error.

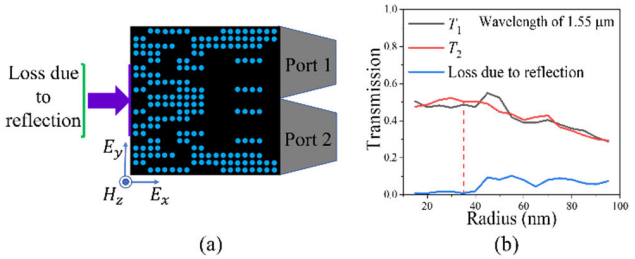

FIGURE 2. (a) A power splitter with hole (SiO_2) configuration corresponding to equal splitting at the output ports, to calculate transmission and reflection loss at different radius; (b) the transmission vs radius curves, where the optimized radius of 35 nm is marked with red dashed line. We defined the figure of merit as FOM = max transmission, ($T_1 + T_2$) – min reflection, (R). Maximum FOM at the wavelength of 1.55 μm is observed at 35 nm. Reflection loss increases after around 35 nm.

From Fig. 2(b), at 35 nm, the reflection loss is minimum (0.008) with a transmittance of 0.99. This estimation has also been performed and validated for 1.45 μm and 1.65 μm and a few other designs (not shown in Fig. 2). This indicates that a hole radius of around $\lambda/40$ should provide optimum performance.

C. MATERIALS AND MODES DEPENDENT TOTAL TRANSMISSION

Next, the total transmissions for the 16,000 random structures, are shown in Fig. 3 for TE and TM mode.

Transmission = P_{out}/P_{in} has been calculated where P_{in} designates the input power through port 1 and P_{out} as the total transmitted power from the two output ports. Transmission over the whole frequency range of 1.45 μm to 1.65 μm, which is the most used band for optical communication, is shown in Fig. 3(a).The maximum and minimum change from the central wavelength is only 0.27% (Si_3N_4) and 2% (SiO_2) respectively. This variation being very low indicates the fact

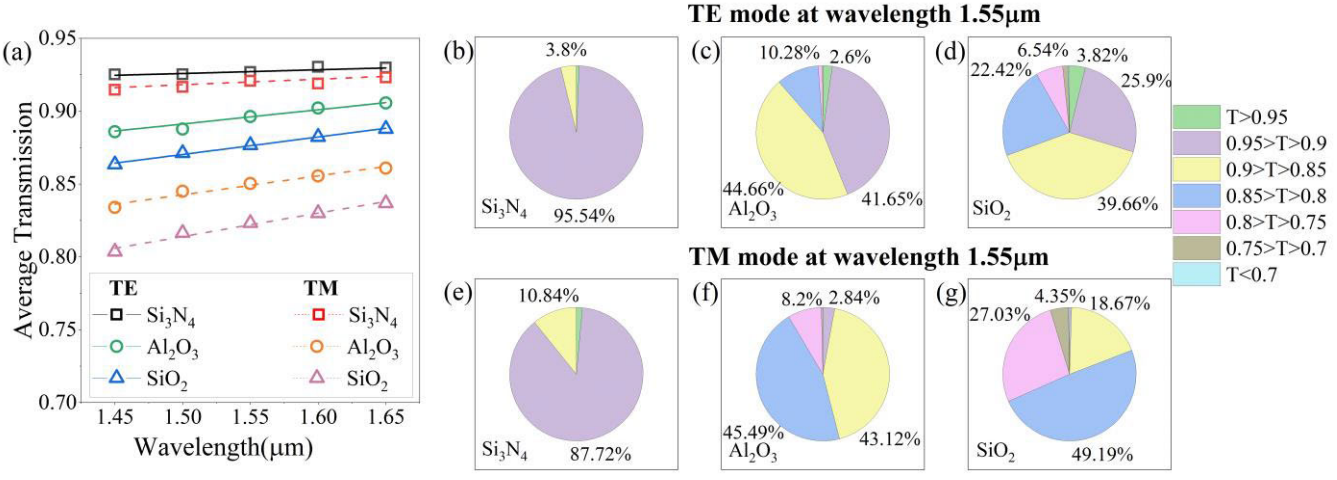

FIGURE 3. (a) Average transmission for 16 thousand random configurations at the wavelength range of 1.45 μm to 1.65 μm for TE (solid lines) and TM (dashed lines) modes. Total transmission of the random configurations for (b)-(d) TE and (e)-(g) TM mode, and for 3 dielectric materials of (b), (e) Si_3N_4, (c), (f) Al_2O_3, and (d), (g) SiO_2 as holes at the center wavelength of 1.55 μm.

that the response of the representative data for the center frequency of 1.55 μm can be chosen for further analysis. The probability of higher transmission is found when the TE mode (Fig. 3(b) –(d)) is applied, in comparison to the TM mode (Fig. 3(e) –(g)) as a source.

D. MATERIAL AND TRANSMISSION MODE DEPENDENT SPLITTING RATIO (SR)

To investigate the effects of TE and TM modes for different hole materials on a larger scale, splitting ratios are calculated for all 16,000 unique structures. Fig. 4(a) and (b) represent the percentage of occurrence of SRs, for 3 different dielectric materials at both fundamental modes. Here, the splitting ratio (SR) is defined in (1).

$$SR = \frac{T_1}{T_1 + T_2} \tag{1}$$

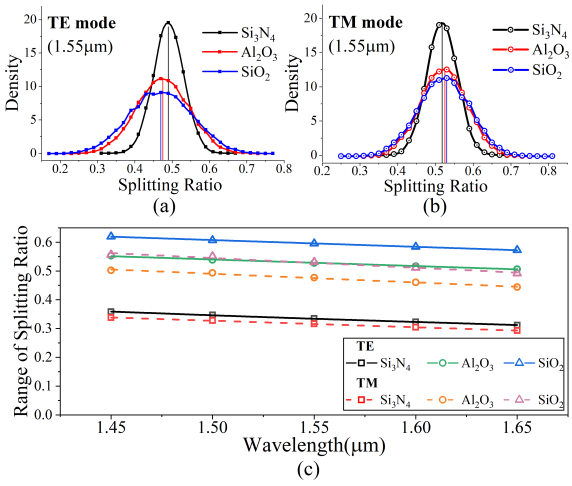

FIGURE 4. Distribution of splitting ratios at 1.55 μm of 16 thousand random configurations for three hole materials, illuminated by two-mode sources, (a) TE and (b) TM. The mean values of the distributions are marked with lines. (c) The dynamic range of splitting ratio (3σ; σ = standard deviation) over the wavelength range of 1.45 μm to 1.65 μm for both TE (solid lines) and TM (dashed lines) displays the smallest range for Si_3N_4, then for Al_2O_3 and the largest range in SiO_2.

The peaks of the curves in Fig. 4(a) and (b) show that TE mode structures are more inclined toward SR < 0.5 and TM mode structures toward SR > 0.5 at the central wavelength. This indicates that in TE polarization, enhanced propagation occurs towards port 2, while for TM, port 1 is more favorable. This trend is evident in 60% of the structures, irrespective of hole materials. If we define the dynamic range of SR by 3σ deviation (σ being the standard deviation of the distribution) from the corresponding mean, covering 99.7% of the data, there is a gradual increase from 0.33 for Si_3N_4, 0.53 for Al_2O_3 to most variation or highest dynamic range of SR for SiO_2 which is 0.6 for TE mode source.

Another observation from the curves of Fig. 4(a) and (b) is that, compared to SiO_2 and Al_2O_3, Si_3N_4 has the narrowest range of SR, suggesting most of the ratios are near the peak. Also, for Si_3N_4, as verified by thousands of random

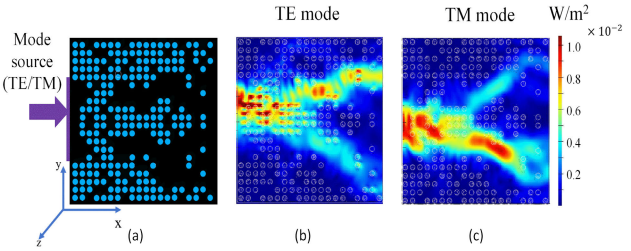

FIGURE 5. (a) A random hole distribution of a photonic power splitter with optimized radius, (b) and (c) Poynting vector corresponding to the structure in (a) with mode source of TE and TM respectively.

configurations, the ratios vary the least with the change of configurations.

Dynamic ranges are also recorded for the overall bandwidth of 200 nm (Fig. 4(c)). Upon obtaining linear fittings of the data points, the slopes obtained for TE and TM polarization are around 0.23 for all three materials. Again, negligible frequency dependency is observed within the range, justifying our selection of single-center frequency for further rigorous analysis. The lower dynamic range of power distribution occurs due to the small difference in refractive indices between Si and Si_3N_4. For TM mode source, structures have a slightly lower range for all materials compared to their corresponding TE mode structures in the concerned window.

The power distribution ratio between the two ports mainly depends on the effective length of the coupled region i.e., the splitter geometry, branching angles towards two ports, and the optical properties of the materials. Divergence near the output ports adds excess attenuation, by introducing local mode to the radiating field. Hence, TE and TM modes at the same frequency incorporate different propagation vectors with varying splitting ratios. For a random structure, as shown in Fig. 5(a), the typical power flow distribution for both TE and TM mode are provided in Fig. 5(b) and (c), respectively. Here, holes of SiO_2 with optimized radius are implemented where, splitting ratio (SR) (defined in eq. (1)) is 0.61 for TE mode, and for TM mode, it is 0.33. The coupling ratio between the two output ports occurs in M:N form, where M and N take any value from 1 to 5.

E. SENSITIVITY TO FABRICATION ERROR

Complex fabrication processes, for example, during etching, can sometimes lead to additional or missing holes. To investigate which locations of the holes are more sensitive to fabrication errors, we select a base random structure and then toggle the hole at each position, to see its impact on the output transmission. The hole toggle means turning each matrix position ON (hole present), if there is no hole at that position, or OFF (hole absent), when there is a hole present, one at a time.

It is to be noted that all three dielectric materials are shown in Fig. 6 (a) have the same base random structure, each having 400 data points for the 20×20 matrix. The same observations were found with few other random structures. In all cases,

TABLE 2. Comparison of previously reported photonic crystal power splitter.

Year (Ref)	Dimension (μm×μm)	Average Transmission (%)	Hole Distribution	Hole dimension (nm)	Materials used
2013 [19]	10×8	100	Controlled/ Systematic	128 (Uniform)	Si-GaAs (Triangular lattice)
2019 [31]	2.6×2.6	90	Random	45 (Uniform)	Si-SiO_2 (Square lattice)
2020 [33]	10×10	97	Controlled/ Systematic	370 (Uniform)	Si-Air- defect rods at the bend (Hexagonal lattice)
2020 [32]	2.25×2.25	91.8	Random	40 to 72 (Non-Uniform)	Si-SiO_2 (Square lattice)
Proposed	2×2	94.935	Random	35 (Uniform)	Si- SiO_2, Si-Al_2O_3, Si-Si_3N_4 (Square lattice)

most configurations followed the base SR ratio, and those that varied most are considered as the ''outliers''. Hence, those positions of the outlier holes are mostly sensitive to fabrication uncertainties. The positions responsible for outliers (points beyond σ distribution from the mean) are highlighted in the square structures representing the power splitter and are shown in the inset of Fig. 6(a). A significant observation from the patterns is that the outliers are mostly near the edge of the device where the source is positioned, irrespective of materials; this necessitates careful considerations to avoid any fabrication defects close to the source.

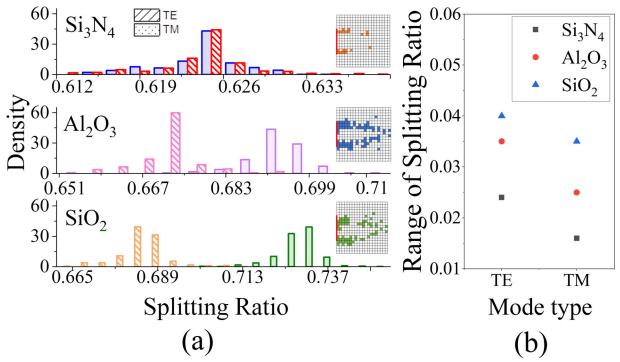

FIGURE 6. (a) Occurrence of splitting ratio (SR), as defined in (1), with hole toggling for three dielectric materials, (b) dynamic ranges of SR at different modes. Significant outlier positions (beyond σ distribution from the mean) for each material are highlighted in the schematic structures in the inset of (a). The source is shown with the red line on the surface.

The dynamic range of SR (defined as 3σ to -3σ distribution from mean) extracted from Fig. 6(a), is shown in Fig. 6(b). Considering minimum error occurring in one-hole position at a time, Fig. 6(b) shows that the lowest variation of SR (dynamic range of SR) is obtained when holes are made of Si_3N_4. Also, the structure is least tolerant to fabrication errors for SiO_2 and most tolerant for Si_3N_4 holes.

F. COMPARISON WITH PREVIOUSLY REPORTED PHOTONIC POWER SPLITTERS

The performance of our proposed design is compared with previously reported power splitters with photonic crystal in the Table 2. As observed from the table, the structures having controlled or systematic hole (or rod for 2D photonic crystal) distribution, rather than random distribution as in this work, [19], [33] show higher average transmission than our structure. But for such systematic distribution, structures with much larger dimensions are required, to prevent sharp bending angles. Hence, all the structures in [19], [33] have a significantly larger size compared to the randomly distributed ones. Also, losses due to sharp bending can be avoided by placing randomly distributed holes. Among the randomly distributed power splitters, our proposed structure is of the smallest dimensions reported up to date with the higher average transmission of 94.935% for equally power splitting configuration compared to the transmission reported by [31], [32] in recent times.

III. FORWARD MODELING FOR 1.55 μm OPTICAL POWR SPLITTER

Next, we use the ML algorithm to perform forward modeling analysis only on the dataset for the splitter with hole material made up of Si_3N_4, consisting of 16 thousand random configurations. Here, our predictions of transmission response for arbitrary Hole Vector (HV) structures are based on the device working at 1.55 μm and bandwidth ranging from 1.45 to 1.65 μm. For this purpose, LM and ANN were used to build the regressors for a forward model. We found that the prediction of transmission response could be done using a shallow ANN, and the LM made marginally better predictions compared to the ANN. In the following subsections, we present the implementation details of our ML pipeline followed by the forward modeling performance results.

A. DATASET

As stated in the previous sections, the dataset for dielectric material of Si_3N_4 has a total of 16,000 HV structures, where each of the HV containing $\mathbb{R}^{400}$ binary input features, represents a unique 20 × 20 HV structure. The problem is constructed as a regression task, where the T_1 and T_2 transmissions for an arbitrary HV structure were predicted. The reflection loss (R) of the HV is not included in the prediction as it can be calculated easily from (2) and it also simplified our regression task as well.

$$T_1 + T_2 + R = 1 \tag{2}$$

The dataset was randomly split between the train and test sets using a stratified sampling method, to a ratio of 80:20. No standardization or normalization operation was performed on the dataset after splitting, as preprocessing did not increase our model performance. We also performed a 5-fold Cross-validation with 3 repeats. However, the results of the repeated k-Fold Cross-Validation were found to be the same as a single train-test split. Therefore, we have only reported the results of a single split. The train test split was done using the *R* package *splitTools*.

B. IMPLEMENTATION DETAILS

The LM was implemented using base $\mathbb{R}$. T_1 and T_2 were predicted using the 400 HV inputs. The linear equations of LM are

$$Y_{T_1} = \beta_{0T_1} + X.\beta_{T_1} \tag{3}$$
$$Y_{T_2} = \beta_{0T_2} + X.\beta_{T_2} \tag{4}$$

where, Y_{T_1}, Y_{T_2} represent the predicted transmittance and β_{0T_1} and β_{0T_2} indicate the intercept terms for T_1 and T_2 respectively. X along with β_{T_1} and β_{T_2} are 400-length single vectors that contain all HV inputs and all the corresponding coefficients to the HV positions respectively.

The ANN was implemented in Keras, where a shallow network was used for the prediction purpose that consisted of only 2 hidden layers.

As input, 400 HV positions were used. Our output consisted of 2 neurons, each predicting T_1 and T_2 respectively. We used the He uniform initialization [34] to initialize our hidden layers. Both *sigmoid* and *tanh* were found to be a viable option as activation function, where, *sigmoid* took longer to train compared to *tanh*. However, we used *ReLU* (Rectified Linear Unit) as our activation function as it converged the fastest compared to *sigmoid* and *tanh*.

We did not use any input normalization (*BatchNorm*) for our hidden layers [35] as it did not increase the model performance. We used *Adam* [36] as our optimizer with a fixed Learning Rate (LR) of 0.005 and epsilon of 0.0003. The model was trained for 25 epochs with a batch size of 100. Also, 20% of our training set was used as a validation set.

TABLE 3. Forward modeling performance of LM and ANN.

	T_1		T_2	
	LM	ANN	LM	ANN
RMSE	0.0075	0.0103 ±0.002	0.0076	0.0115 ±0.003
RMSPE (%)	0.0167	0.0229 ±0.004	0.0162	0.0244 ±0.006
MAE	0.0059	0.0082 ±0.002	0.0059	0.0093 ±0.003
MAEPE (%)	0.0131	0.0181 ±0.004	0.0127	0.0197 ±0.006

C. FORWARD MODELING PERFORMANCE

The forward modeling performances of the models are given in Table 3, where ± indicates the standard deviation. To validate our ANN results, we use 10 different random seeds. The LM performed marginally better for both T_1 and T_2 prediction

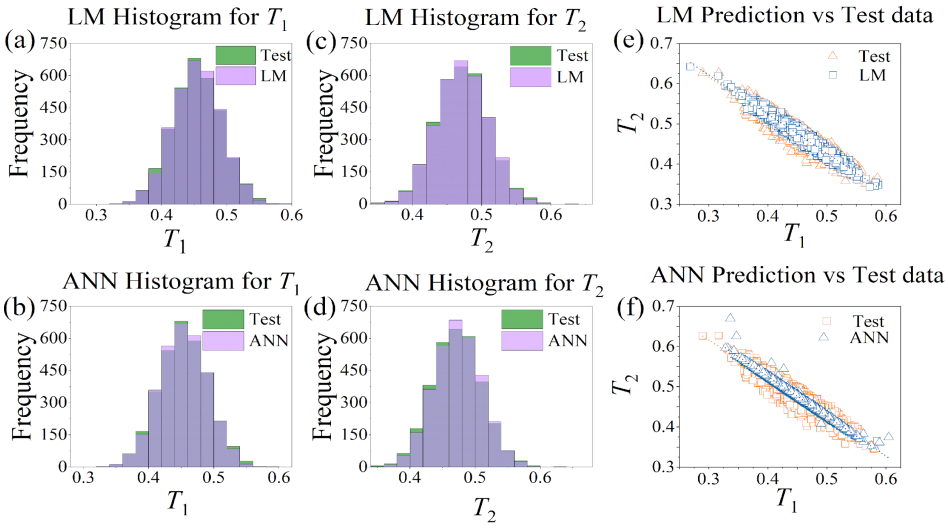

FIGURE 7. Comparison of LM and ANN predictions. (a), (c) is the overlay of Test and LM predicted T_1 and T_2, (e) is fitting of LM predicted T_1 vs T_2 on Test T_1 vs T_2. (b), (d) is the overlay of Test and ANN predicted T_1 and T_2 (f) is fitting of LM predicted T_1 vs T_2 on Test T_1 vs T_2.

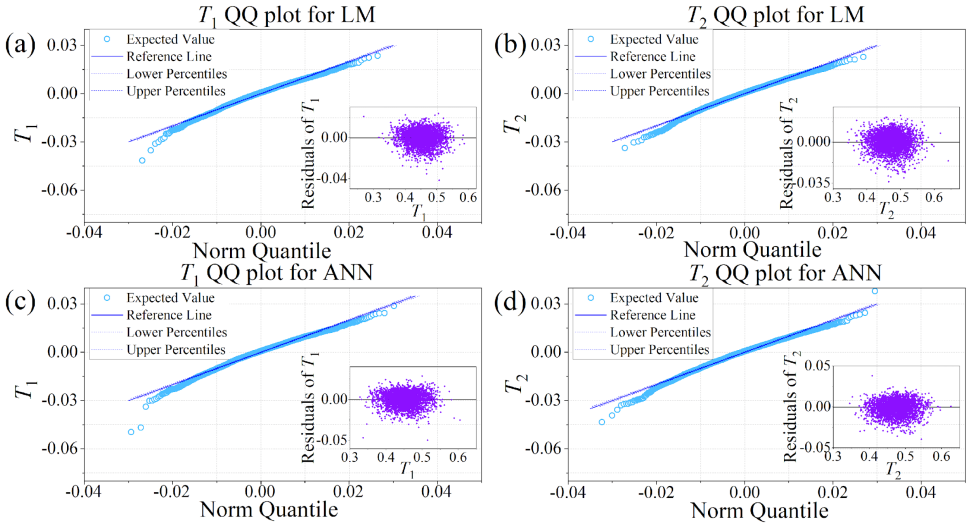

FIGURE 8. QQ plot of residuals and residual vs fitted plots (inset) for LM and ANN.

compared to the ANN. Fig. 7 shows the comparison between test vs predicted results.

While predicting T_1 in Fig. 7(a) and 7(b), both LM and ANN had an error on the mean region (0.44-0.46) of the test set. However, the ANN made more errors around the mean (0.40 to 0.44 and 0.46 to 0.48) compared to the LM, by predicting more values as per count frequency than the test set. Similar behavior can be observed in LM for T_1 prediction (0.46 to 0.48). The same trend for errors is observed in Fig. 7(c) and 7(d), from both LM and ANN. However, for T_2, both models made errors mostly around the mean. Again, as seen for T_1 the ANN made more errors due to more prediction as per count frequency. From Fig. 7(e) and 7(f), we can see that the predicted values of the LM have more variance compared to the ANN predictions respectively.

Fig. 8 shows the QQ plot for our prediction residuals and the residual vs fitted plot for LM (Fig. 8(a)- (b)) and ANN (Fig. 8(c)-(d)). From the QQ plot, we can see that compared to LM the prediction residuals for ANN deviate more in the lower quantile for T_1 and in the upper quantile for T_2. We found that a residual of ± 0.02 for both T_1 and T_2 kept our SR error under 5%, which can be observed in the residual vs fitted plot.

We also visualized the structure of our device, with the coefficients of the hole vector positions of our LM in Fig 9. The brighter regions mean that these coefficient values are more influential in the prediction of respective transmittance, given there is a hole in that region. This can be interpreted as the importance of hole vector position in a configuration.

From Fig. 9, the most significant areas are found to be at the source edges, which agrees with our observation from FDTD simulations in Fig. 6. Interestingly, the upper port (T_1) gets more influenced by the lower edge of the source, and vice versa for the lower port (T_2). This is because the light from the source edge that lies diagonally to the output port has to

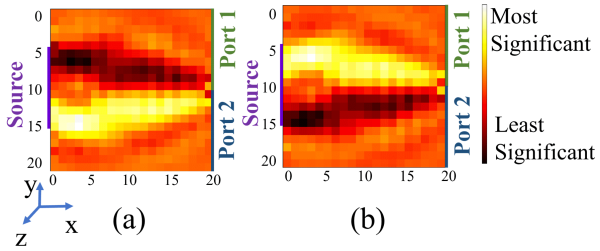

FIGURE 9. The structure of the photonic power splitter with the coefficients of the LM is a 20 × 20 matrix, where each 1 × 1 index corresponds to the coefficients. This representation also shows the importance of HV with respect to the coefficients for both (a) T_1 and (b) T_2.

cover a further distance than the closer one. Therefore, adding any obstacles (holes) into the longer path will create more disturbance than the shorter one.

We found that the LM performed marginally better compared to the ANN in the single transmittance prediction. We believe this is due to the nature of the forward modeling problem. ANNs seem to slightly overfit the problem which in terms reduces their prediction quality compared to LM. We believe using single-layer ANNs with regularizations should solve this issue.

From this analysis, we verify that it is possible to do forward modeling using a single wavelength response. For most DL-based inverse modeling, meaning predicting a topology for a target optical response [37]–[41], broadband spectrum is required. It is to note that, to construct an inverse model, forward modeling solutions are crucial building blocks for tandem networks [37], [42], [43] and iterative methods [22], [44]–[46]. Hence, we solely focus on the forward modeling here and inverse design remains beyond the scope of this study. We also believe that our dataset can be used for inverse modeling for Generative model-based

solutions like variants of Generative Adversarial Network (GAN) [38] and Variational Autoencoder (VAE) [37], [39].

IV. CONCLUSION

A 1 × 2 compact footprint of 2 μm × 2 μm power splitter offering an arbitrary splitting ratio in the popular optical communication spectrum around 1.55 μm has been proposed. To obtain a wide span of transmittance values particularly from 0.75 to 0.95, a random pattern of holes was etched onto the silicon substrate and 16,000 unique designs are generated for the study. Dimension of the holes are optimized ensuring minimum reflection losses and the effect of different materials have also been investigated. It is observed that the Si_3N_4-Si combination offers the highest and most stable transmittance response making it the least sensitive to fabrication uncertainties. To be specific, 96% of structures with Si_3N_4 holes show minimum transmission of 90% compared to 26% of structures with SiO_2 holes. The coupling ratio between the two output ports is M:N, where M and N vary from 1 to 5. achieved for 3 different dielectric materials: SiO_2, Al_2O_3, and Si_3N_4. Modal analysis indicates that better transmittance is evident for TE mode at 1.55 μm. Machine learning has also been adopted to accurately predict the transmittances of any possible design of the structure. Both LM and ANN have been incorporated for this forward model. However, LM shows better accuracy in terms of RMSE value of only 0.84%. The model clearly shows that the hole vectors in the lower half of the splitter make a higher contribution in the transmittance of the upper port and vice versa. To the best of the author's knowledge, such comprehensive analysis has not been reported yet, which can pave the way for realizing compact and efficient photonic power splitters. The data used in this work are freely available for any future analysis.

ACKNOWLEDGMENT

The authors thank the technical support from Fab Laboratory DU at the University of Dhaka and the Bangladesh Research and Education Network (BdREN) for providing the necessary computational resources for this simulation study. They would also like to thank Ibraheem Muhammad Moosa and Imtiaz Ebna Mannan for providing valuable insight for Section III and Mohammad Atiqul Islam for helping with the graphical abstract (GA).

REFERENCES

[1] J. Goodman, F. Leonberger, and S. Kung, "Optical interconnections for VLSI systems," in *Proc. IEEE*, vol. 72, no. 7, pp. 850–866, Jul. 1984, doi: 10.1109/PROC.1984.12943.

[2] R. G. Hunsperger, *Integrated Optics*. New York, NY, USA: Springer, 2009, doi: 10.1007/b98730_1.

[3] A. Polman, M. Kociak, and F. J. García de Abajo, "Electron-beam spectroscopy for nanophotonics," *Nature Mater.*, vol. 18, no. 11, pp. 1158–1171, Nov. 2019, doi: 10.1038/s41563-019-0409-1.

[4] S. Fan, "An alternative 'sun' for solar cells," *Nat Nanotech.*, vol. 9, pp. 92–93, Feb. 2014, doi: 10.1038/nnano.2014.9.

[5] Y. Wang, P. Wang, X. Zhou, C. Li, H. Li, X. Hu, F. Li, X. Liu, M. Li, and Y. Song, "Diffraction-grated perovskite induced highly efficient solar cells through nanophotonic light trapping," *Adv. Ener. Mat.*, vol. 8, no. 12, Jan. 2018, Art. no. 1702960, doi: 10.1002/aenm.201702960.

[6] M. Naruse, N. Tate, M. Aono, and M. Ohtsu, "Information physics fundamentals of nanophotonics," *Rep. Prog. Phys.*, vol. 76, no. 5, Apr. 2013, Art. no. 056401, doi: 10.1088/0034-4885/76/5/056401.

[7] L. Mu, Y. Chang, S. D. Sawtelle, M. Wipf, X. Duan, and M. A. Reed, "Silicon nanowire field-effect transistors—A versatile class of potentiometric nanobiosensors," *IEEE Access*, vol. 3, pp. 287–302, 2015, doi: 10.1109/ACCESS.2015.2422842.

[8] S. Assefa, F. Xia, and Y. A. Vlasov, "Reinventing germanium avalanche photodetector for nanophotonic on-chip optical interconnects," *Nat. Lett.*, vol. 464, pp. 80–84, Mar. 2010, doi: 10.1038/nature08813.

[9] X. Li, H. Xu, X. Xiao, Z. Li, J. Yu, and Y. Yu, "Compact and low-loss silicon power splitter based on inverse tapers," *Opt. Lett.*, vol. 38, no. 20, pp. 4220–4223, Oct. 2013, doi: 10.1364/OL.38.004220.

[10] P. Velha, V. Sorianello, M. V. Preite, G. De Angelis, T. Cassese, A. Bianchi, F. Testa, and M. Romagnoli, "Wide-band polarization controller for Si photonic integrated circuits," *Opt. Lett.*, vol. 41, no. 24, pp. 5656–5659, Dec. 2016, doi: 10.1364/OL.41.005656.

[11] K. Kishioka, "A design method to achieve wide wavelength-flattened responses in the directional coupler-type optical power splitters," *J. Lightw. Technol.*, vol. 19, no. 11, pp. 1705–1715, Nov. 2001, doi: 10.1109/50.964071.

[12] C. R. Doerr, N. K. Fontaine, and L. L. Buhl, "PDM-DQPSK silicon receiver with integrated monitor and minimum number of controls," *IEEE Photon. Technol. Lett.*, vol. 24, no. 8, pp. 697–699, Apr. 15, 2012, doi: 10.1109/LPT.2012.2187048.

[13] J. Sun, E. Timurdogan, A. Yaacobi, E. S. Hosseini, and M. R. Watts, "Large-scale nanophotonic phased array," *Nature*, vol. 493, no. 7431, pp. 195–199, Jan. 2013, doi: 10.1038/nature11727.

[14] H. Xu and Y. Shi, "Ultra-broadband dual-mode 3-dB power splitter based on a Y-junction assisted with mode converters," *Opt. Lett.*, vol. 41, no. 21, pp. 5047–5050, Nov. 2016, doi: 10.1364/OL.41.005047.

[15] T. Liu, A. R. Zakharian, M. Fallahi, J. V. Moloney, and M. Mansuripur, "Multimode interference-based photonic crystal waveguide power splitter," *J. Lightw. Technol.*, vol. 22, no. 12, pp. 2842–2846, Dec. 2004, doi: 10.1109/JLT.2004.834479.

[16] Q. Deng, L. Liu, X. Li, and Z. Zhou, "Arbitrary-ratio 1×2 power splitter based on asymmetric multimode interference," *Opt. Lett.*, vol. 39, no. 19, pp. 5590–5593, Oct. 2014, doi: 10.1364/OL.39.005590.

[17] H. Xu, D. Dai, and Y. Shi, "Ultra-broadband on-chip multimode power splitter with an arbitrary splitting ratio," *OSA Continuum*, vol. 3, no. 5, pp. 1212–1221, May 2020, doi: 10.1364/OSAC.396024.

[18] K. K. Chung, H. P. Chan, and P. L. Chu, "A 1×4 polarization and wavelength independent optical power splitter based on a novel wide-angle low-loss Y-junction," *Opt. Commun.*, vol. 267, no. 2, pp. 367–372, Nov. 2006, doi: 10.1016/j.optcom.2006.06.048.

[19] R. Ahmed, M. M. Khan, R. Ahmmed, and A. Ahad, "Design, simulation & optimization of 2D photonic crystal power splitter," *Opt. Photon. J.*, vol. 3, no. 2, pp. 13–19, 2013, doi: 10.4236/opj.2013.32A002.

[20] K. Hornik, M. Stinchcombe, and H. White, "Multilayer feedforward networks are universal approximators," *Neural Netw.*, vol. 2, no. 5, pp. 359–366, Dec. 1989, doi: 10.1016/0893-6080(89)90020-8.

[21] Z. A. Kudyshev, A. V. Kildishev, V. M. Shalaev, and A. Boltasseva, "Machine learning–assisted global optimization of photonic devices," *Nanophotonics*, vol. 10, no. 1, pp. 371–383, Oct. 2020, doi: 10.1515/nanoph-2020-0376.

[22] Y. Li, Y. Wang, S. Qi, Q. Ren, L. Kang, S. D. Campbell, P. L. Werner, and D. H. Werner, "Predicting scattering from complex nanostructures via deep learning," *IEEE Access*, vol. 8, pp. 139983–139993, 2020, doi: 10.1109/ACCESS.2020.3012132.

[23] R. Selle, T. Brixner, T. Bayer, M. Wollenhaupt, and T. Baumert, "Modelling of ultrafast coherent strong-field dynamics in potassium with neural networks," *J. Phys. B, At. Mol. Opt. Phys.*, vol. 41, no. 7, Mar. 2008, Art. no. 074019.

[24] M. V. Zhelyeznyakov, S. L. Brunton, and A. Majumdar, "Deep learning to accelerate Maxwell's equations for inverse design of dielectric metasurfaces," 2020 *arXiv:2008.10632*.

[25] M. M. R. Elsawy, S. Lanteri, R. Duvigneau, J. A. Fan, and P. Genevet, "Numerical optimization methods for metasurfaces," *Laser Photon. Rev.*, vol. 14, no. 10, Oct. 2020, Art. no. 1900445, doi: 10.1002/lpor.201900445.

[26] E. Bor, M. Turduev, and H. Kurt, "Differential evolution algorithm based photonic structure design: Numerical and experimental verification of subwavelength λ/5 focusing of light," *Sci. Rep.*, vol. 6, Aug. 2016, Art. no. 30871, doi: 10.1038/srep30871.

[27] *The Dataset*. Accessed: Nov. 15, 2022. [Online]. Available: https://github.com/mandelbrot-walker/Photonic-pspliiter-fm
[28] A. D'Amour, K. Heller, D. Moldovan, and B. Adlam, "Underspecification presents challenges for credibility in modern machine learning," 2020, *arXiv:2011.03395*.
[29] B. Schauwecker, M. Arnold, C. Radehaus, G. Przyrembel, and B. Kuhlow, "Optical waveguide components with high refractive index difference in silicon-oxynitride for application in integrated optoelectronics," *Opt. Eng.*, vol. 41, no. 1, pp. 237–243, Jan. 2002, doi: 10.1117/1.1419188.
[30] R. A. Soref, S. J. Emelett, and W. R. Buchwald, "Silicon waveguided components for the long-wave infrared region," *J. Opt. A, Pure Appl. Opt.*, vol. 8, no. 10, pp. 840–848, Oct. 2006, doi: 10.1088/1464-4258/8/10/004.
[31] H. Mohammad Tahersima, K. Kojima, T. Koike-Akino, D. Jha, B. Wang, C. Lin, and K. Parsons, "Deep neural network inverse design of integrated photonic power splitters," *Sci. Rep.*, vol. 9, Feb. 2019, Art. no. 1368, doi: 10.1038/s41598-018-37952-2.
[32] Y. Tang, K. Kojima, T. Koike-Akino, Y. Wang, P. Wu, M. Tahersima, D. Jha, K. Parsons, and M. Qi, "Generative deep learning model for a multi-level nano-optic broadband power splitter," in *Proc. Opt. Fib. Commun. Conf. (OFC)*, San Diego, CA, USA, Mar. 2020, pp. 1–5, doi: 10.1364/OFC.2020.Th1A.1.
[33] H. Kaur and P. Jindal, "A compact polarization independent power splitter for mid ir range," *IOP Conf. Mat. Sci. Engi.*, vol. 993, Oct. 2020, Art. no. 012118, doi: 10.1088/1757-899X/993/1/012118.
[34] K. He, X. Zhang, S. Ren, and J. Sun, "Delving deep into rectifiers: Surpassing human-level performance on imagenet classification," in *Proc. IEEE Int. Conf. Comp. Vis. (ICCV)*, Feb. 2015, pp. 1026–1034, doi: 10.1109/ICCV.2015.123.
[35] S. Ioffe and C. Szegedy, "Batch normalization: Accelerating deep network training by reducing internal covariate shift," in *Proc. 32nd Int. Conf. ML (PMLR)*, vol. 37, 2015, pp. 448–456.
[36] D. P. Kingma and J. Ba, "Adam: A method for stochastic optimization," in *Proc. 3rd Int. Conf. Learn. Represent.*, 2015, pp. 1–5.
[37] S. So, J. Mun, and J. Rho, "Simultaneous inverse design of materials and structures via deep learning: Demonstration of dipole resonance engineering using core–shell nanoparticles," *ACS Appl. Mater. Interface*, vol. 11, no. 27, pp. 24264–24268, Jun. 2019, doi: 10.1021/acsami.9b05857.
[38] S. So and J. Rho, "Designing nanophotonic structures using conditional deep convolutional generative adversarial networks," *Nanophotonics*, vol. 8, no. 7, pp. 1255–1261, Jun. 2019, doi: 10.1515/nanoph-2019-0117.
[39] Z. Liu, L. Raju, D. Zhu, and W. Cai, "A hybrid strategy for the discovery and design of photonic structures," *IEEE J. Emerg. Sel. Topics Circuits Syst.*, vol. 10, no. 1, pp. 126–135, Mar. 2020, doi: 10.1109/JETCAS.2020.2970080.
[40] M. Turduev, E. Bor, C. Latifoglu, I. H. Giden, Y. S. Hanay, and H. Kurt, "Ultracompact photonic structure design for strong light confinement and coupling into nanowaveguide," *J. Lightw. Technol.*, vol. 36, no. 14, pp. 2812–2819, Jul. 15, 2018, doi: 10.1109/JLT.2018.2821361.
[41] J. Jiang and J. A. Fan, "Global optimization of dielectric metasurfaces using a physics-driven neural network," *Nano Lett.*, vol. 19, no. 8, pp. 5366–5372, Jul. 2019, doi: 10.1021/acs.nanolett.9b01857.
[42] D. Liu, Y. Tan, E. Khoram, and Z. Yu, "Training deep neural networks for the inverse design of nanophotonic structures," *ACS Photon.*, vol. 5, no. 4, pp. 1365–1369, Feb. 2018, doi: 10.1021/acsphotonics.7b01377.
[43] W. Ma, F. Cheng, and Y. Liu, "Deep-learning-enabled on-demand design of chiral metamaterials," *ACS Nano*, vol. 12, no. 6, pp. 6326–6334, 2018.
[44] T. Asano and S. Noda, "Iterative optimization of photonic crystal nanocavity designs by using deep neural networks," *Nanophotonics*, vol. 8, no. 12, pp. 2243–2256, Nov. 2019, doi: 10.1515/nanoph-2019-0308.
[45] A. Sheverdin, F. Monticone, and C. Valagiannopoulos, "Photonic inverse design with neural networks: The case of invisibility in the visible," *Phys. Rev. A, Gen. Phys.*, vol. 14, no. 2, Aug. 2020, Art. no. 024054, doi: 10.1103/PhysRevApplied.14.024054.
[46] A. P. Blanchard-Dionne and O. J. F. Martin, "Successive training of a generative adversarial network for the design of an optical cloak," *OSA Contin.*, vol. 4, no. 1, pp. 87–95, Jan. 2021, doi: 10.1364/OSAC.413394.

LUBABA TAZRIAN RAHMAN received the B.Sc. degree in electrical and electronic engineering, with the major in electronics from the University of Dhaka, Bangladesh, in 2019, where she is currently pursuing the M.Sc. degree in electrical and electronic engineering, with the major in applied physics.

She had experience as an Intern, in 2018, with Dhaka Power Distribution Company (DPDC) in the 1st GIS distribution substation in Bangladesh where she had to prepare field observation reports about the details of some protection schemes, relay system, interlock system, and their applications in the distribution substation. Her current research interests include nanoscale electronic and optoelectronic devices and their app locations, biosensors, inverse design of nanophotonic devices, and hybrid power system in remote areas for utilizing renewable energy.

Ms. Rahman is also a Student Member of the Optical Society of America (OSA).

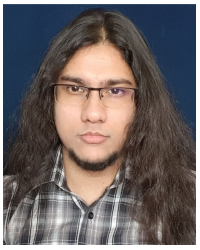

MAHMUD ELAHI AKHTER is currently pursuing the bachelor's degree in computer science and engineering with North South University.

He is also a Research Assistant at the Department of Electrical and Computer Engineering, North South University, and the Institute of Statistical Research and Training, University of Dhaka. His research interests include complex analysis, stochastic optimization, computational biology, explainable (XAI) and interpretable AI, computer vision, and natural language processing. His current work focuses on multilingual language models for low-resource languages and the Clever Hans effect in biomedical deep learning models.

FAIZUL RAKIB SAYEM is currently pursuing the bachelor's degree in computer engineering with the Department of Electrical and Electronic Engineering, University of Dhaka, Bangladesh.

He has coauthored three international conference publications. He was the Webmaster (Technical) of IEEE SBDU, in 2020. His research interests include applied machine learning, human–computer interaction, wearable and ubiquitous computing, artificial intelligence applications in nanophononics, computer vision, signal and image processing, and pattern recognition. He has won a prestigious International Competition (3rd Nurse Care Activity Recognition Challenge) which is held as a part of Hasca Workshop in ACM UbiComp 2021. He has also achieved the Best Paper Award (Bronze Edition) at 10th ICIEV, 2021.

MAINUL HOSSAIN (Member, IEEE) received the Ph.D. degree in electrical engineering from the University of Central Florida, Orlando, FL, USA, in 2012.

From 2012 to 2017, he worked as a Principal Engineer with the Advanced Module Engineering (AME) Department, Globalfoundries US Inc., Malta, NY, USA, where he was responsible for developing state-of-the-art metrology solutions for 14 nm and beyond technology nodes. He joined the University of Dhaka, in 2017, where he is currently an Assistant Professor with the Department of Electrical and Electronic Engineering. He holds one U.S. patent and has coauthored one book chapter and more than 25 research articles in reputed journals. His current research interests include emerging nanoscale electronic and optoelectronic devices for low power computing, biosensing, and energy harvesting.

Dr. Hossain is a member of the National Young Academy of Bangladesh (NYAB) and the Faculty Advisor of Optica (formerly OSA) Bangladesh Chapter at the University of Dhaka and the IEEE EDS Student Branch Chapter at the University of Dhaka.

RAJIB AHMED is currently a Research Fellow at the School of Medicine, Stanford University, and the Canary Center at Stanford for Cancer Early Detection. His optics and biosensing research have been widely published over 100 scientific publications. His current research interests include micro- and nanotechnology to create inexpensive optical devices for biomedical applications. He is a contributing editor and a reviewer for numerous scientific journal communities.

M. M. LUTFE ELAHI received the M.Sc. degree in computer engineering from The University of Texas at Arlington, USA, in 2008.

He is currently a Senior Lecturer with the Department of Electrical and Computer Engineering, North South University, Bangladesh. His current research interests include machine learning and computer vision.

KHALEDA ALI received the M.S. degree from the Department of Electrical and Electronic Engineering, University of Dhaka, in 2006, and the Ph.D. degree from the Department of Electronic Engineering, Queen Mary University of London, in 2014.

She is currently working as an Assistant Professor with the Department of Electrical and Electronic Engineering, University of Dhaka. Her research interests include computational electromagnetics, wireless body area networks, and modeling for radio-channel characterization.

SHARNALI ISLAM received the Ph.D. degree from the University of Illinois at Urbana–Champaign, Champaign, IL, USA, in 2014.

She was the Faculty Group Advisor of the IEEE WIE Student Branch Dhaka University (2018–2019). She is currently an Assistant Professor of electrical and electronic engineering at the University of Dhaka, where she joined, in 2017. Before her career in academia, she was a Device Engineer at Intel Company, USA, working in the NAND Memory Cell Group, defining requirements and roadmap for NAND cell parameters towards meeting the overall technology goal. She has coauthored a book chapter and a total of 23 journal publications in reputed international journals. Her research interests include photonic devices, electrical and thermal modeling of nano-scale computational and energy harvesting devices, and VLSI technology.